Increased Range Bistatic Scatter Radio

John Kimionis, *Student Member, IEEE*, Aggelos Bletsas, *Member, IEEE*, and John N. Sahalos, *Life Fellow, IEEE*

***Abstract*—Scatter radio achieves communication by reflection and requires low-cost and low-power RF front-ends. However, its use in wireless sensor networks (WSNs) is limited, since commercial scatter radio (e.g. RFID) offers short ranges of a few tens of meters. This work redesigns scatter radio systems and maximizes range through non-classic bistatic architectures: the carrier emitter is detached from the reader. It is shown that conventional radio receivers may show a potential 3dB performance loss, since they do not exploit the correct signal model for scatter radio links. Receivers for on-off-keying (OOK) and frequency-shift keying (FSK) that overcome the frequency offset between the carrier emitter and the reader are presented. Additionally, non-coherent designs are also offered. This work emphasizes that sensor tag design should accompany receiver design. Impact of important parameters such as the antenna structural mode are presented through bit error rate (BER) results. Experimental measurements corroborate the long-range ability of bistatic radio; ranges of up to 130 meters with 20 milliwatts of carrier power are experimentally demonstrated, with commodity software radio and no directional antennas. Therefore, bistatic scatter radio may be viewed as a key enabling technology for large-scale, low-cost and low-power WSNs.**

***Index Terms*—Bistatic scatter radio, wireless sensor networks, modulation schemes, software defined radio.**

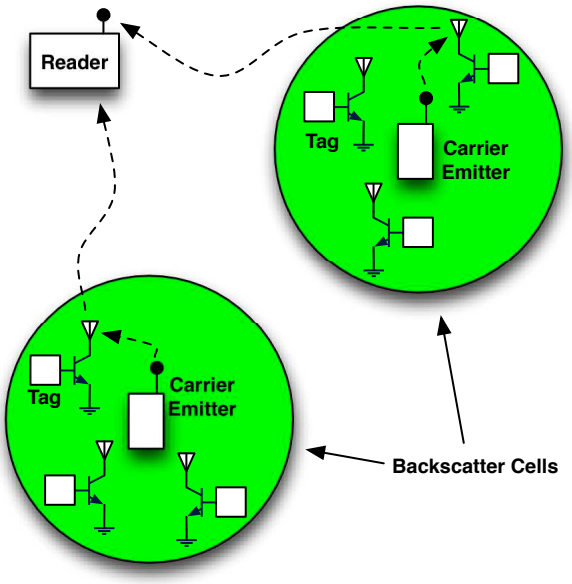

Fig. 1. Backscatter field with sensors/RF tags. Multiple low-cost carrier emitters illuminate tags; a single receiver (reader) is utilized.

I. Introduction

Scatter radio, i.e. communication by means of reflection rather than radiation, although not a new idea (first principles presented in [1]), has only recently been utilized widely for certain applications. The most prominent commercial use of scatter radio is in radio frequency identification (RFID) applications, for identifying people or products in supply chains. Commercial standards have been developed for RFID, albeit focusing on identification/supply chain applications only [2]. However, this communication scheme can be valuable to other scenarios as well, such as in wireless sensor networks (WSNs). Because communication can be achieved with a single radio frequency (RF) transistor front-end, scatter radio can minimize both energy requirements and monetary cost of each sensor node. This allows then for large scale sensor deployments; such networks are critical for applications like precision agriculture, where environmental conditions may have to be measured individually for each plant or among a small group of plants. Recent work has shown proof of concept systems that can be used in dense scatter radio (a.k.a. backscatter radio) networks. All those systems are built with low-cost and low-energy principles in mind [3]–[6].

Extended field coverage is a key characteristic in many WSN applications. This means that the communication range between the sensor *tags* and a *reader* has to be maximized. However, for typical RFID applications, the achieved ranges are inherently limited due to the following:

1) Passive communication; *passive* tags are used, which require energy harvesting to power their electronics. Commonly, these tags rectify a continuous wave (CW) signal, transmitted by the reader. Thus, the achieved range is limited by the so-called "power-up link" [7].

2) High bitrate; commercial RFID systems exploit high bitrates for tag-to-reader communication, on the order of hundreds of kbps, resulting to a small bit duration and thus, reduced energy-per-bit and signal-to-noise ratio (SNR).

3) Monostatic architecture; the reader box consists of both the transmitter that emits the wave needed for backscatter communication and the receiver that decodes the tag-modulated signals. This means that typical RFID systems suffer from round-trip path loss; specifically SNR at the receiver drops with the fourth power of reader-to-tag distance [8] or the eighth power of the distance, for a two-ray propagation model [9], [10]. In monostatic setups, the tags that lay close to the reader are benefitted from the small distance, while tags that lay far are difficult to be "heard" from the reader. This causes a circular area around the reader, where coverage is limited.

For classic monostatic RFID, there are examples in the

This work was supported by the ERC-04-BLASE project, executed in the context of the Education & Lifelong Learning Program of General Secretariat for Research & Technology (GSRT) and funded through European Union-European Social Fund and national funds. Parts of this work previously published at the IEEE RFID-TA 2012, Nice, France, and IEEE GLOBECOM 2013, Atlanta, GA. J. Kimionis and A. Bletsas are with Telecom Lab, ECE Department, Technical Univ. of Crete, Greece, 73100. J. Sahalos is with Radio and Telecommunications Lab, ECE Department, Univ. of Nicosia, Cyprus, 1700. Email:{ikimionis@isc.tuc.gr, aggelos@telecom.tuc.gr, sahalos.j@unic.ac.cy}.

literature that suggest various improvements for the tag-to-reader communication. Work in [11]–[13] focuses on the microwave parameters of the RF tag that impact tag-to-reader communication performance, such as the antenna load selection and the antenna-RFID chip matching. In [14], [15] the authors provide theoretical analysis of multiple input multiple output (MIMO) receivers for the monostatic RFID system. These systems use multiple antennas on the reader to exploit channel diversity for BER reduction. On the other hand, work in [16] utilizes multiple tag antennas to improve the link performance of a 5.8GHz backscatter radio system and [17] studies the multipath fading in such a system. By exploiting multiple tag antennas, the operating ranges are increased up to 78%. However, these ranges are still on the order of a few meters and cannot be efficiently used for long-range sensing.

Therefore, scatter radio has to be redesigned to accommodate WSN applications. To achieve long ranges and extended field coverage, prior art in [3] has directed two key points:

1) Semipassive tags (i.e. energy-assisted) have to be utilized; the tags may power their electronics by batteries or low-cost renewable energy sources like low-voltage solar-cells [18].

2) Bitrate should be minimized, so that energy-per-bit at the receiver is maximized. Although high bitrates are appealing, they are not a necessity for environmental conditions monitoring, because parameters like humidity or temperature change relatively slowly. This allows for smaller duty cycles, with maximized bit durations and longer tag sleep periods to conserve energy.

In this work, a third point is proposed to achieve long range scatter communication for sensor networks. Particularly, *bistatic* architectures should be exploited. By dislocating the carrier emitter from the receiver, new and more flexible topologies can be set up. Carrier emitters may come in the form of an oscillator and a power amplifier only, and can thus be two orders of magnitude cheaper than the receiver/reader. The reader can be a low-cost software defined radio (SDR), which offers the flexibility of processing multiple, arbitrary tag/sensor modulation schemes. One centralized reader may be present at a field, while multiple low-cost carrier emitters can be placed randomly around a field with scattered sensors. That way, the emitter-to-tag path loss can be statistically reduced, since it will be more likely for a tag to lay close to a carrier emitter. Thus, the overall field coverage can be extended, as more emitters are placed around. Such an architecture can be seen in Fig. 1, with multiple carrier emitters and one centralized reader.

It is noted that prior art has largely bypassed bistatic architectures and rather focused on industry-standard monostatic reader architectures. An example towards the bistatic direction is [19] which suggests using a single carrier emitter with multiple receiving-only readers (listeners) that cooperate to decode simultaneously emmiting tags, in an attempt to mitigate interference. Another example of a receiving-only reader is given in [20], where a monitor for commercial-standard Gen2 RFID tags is presented. However, that work does not derive detectors for the tag-to-reader link, but instead exploits heuristic methods of counting pulse durations to determine the transmitted bits. Moreover, the work is tied to the industry-standard FM0 modulation scheme [2]. A recent work utilizing non-conventional backscatter radio communication which exploits ambient RF energy is [21] but that work achieves short ranges since there are no dedicated carrier emitters to feed the tags with sufficient power for long-range sensing.

This work proposes that bistatic architectures are essential for long-range scatter radio and increased area coverage. The contribution of this work is summarized below:

- Design of non-conventional scatter radio system architectures that achieve long ranges of up to 130 meters with 20 milliwatts of carrier power, without directional antennas.
- Derivation of the complete scatter radio signal model, taking into account important microwave parameters that impact tag-to-reader communication performance. It is shown that classic (textbook) receivers do not apply in scatter radio systems, since they do not follow the corresponding signal model and thus may show a 3dB performance loss.
- Noncoherent detectors for the bandwidth-limited (on-off keying-OOK) and the power-limited (frequency shift keying-FSK) regime.
- Demonstrating the importance of overlooked microwave parameters, i.e. the antenna structural mode, on the specific receiver performance, through bit error rate (BER) results.
- Experimental validation of the long-range capability of bistatic links with commodity SDR radio; ranges of up to 130 meters are shown as the proof-of-concept for extended coverage with single-transistor scatter radio.

The rest of this work is organized as follows: Section II derives the complete signal model, Section III describes the scatter links, i.e. tag modulation schemes and corresponding receivers/processing, Section IV analytically calculates the BER for each proposed detector, and Section V offers numerical evaluation. Section VI presents the achieved ranges for outdoor measurements with bistatic setups, and finally Section VII offers the conclusion of this work.

II. System Model

The bistatic scatter radio system consists of a carrier emitter, a sensor tag and a SDR receiver (Fig. 2). The carrier emitter illuminates the RF tag with a continuous wave (CW) carrier at the ultra high frequency (UHF) band. To modulate information, the tag typically terminates its antenna between two loads; in that way, the incident CW is reflected with altered phase and/or amplitude, according to the load that is selected each time. In practice, load switching can be achieved with a single RF transistor, terminating the tag antenna between two loads. Ideally, when the transistor is switched on, the antenna is short-circuited and any incident wave will be scattered back with a negative reflection coefficient (phase change π). Respectively, when the transistor is switched off, the antenna is open-circuited and the incident wave is scattered intact (i.e. no phase change). In this section, the complete signal model for the bistatic link is derived, based on both communication and electromagnetic theory.

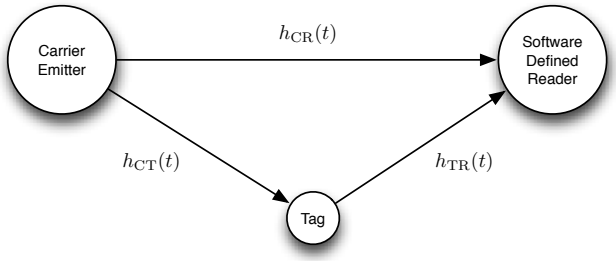

Fig. 2. Bistatic channel model: carrier emitter is dislocated from the receiving reader and RF tag acts as the signal modulator.

We define the *passband* flat-fading channels depicted in Fig. 2:

$$h_{\mathrm{CR}}(t) \triangleq a_{\mathrm{CR}}\ \delta(t-\tau_{\mathrm{CR}}), \tag{1}$$

$$h_{\mathrm{CT}}(t) \triangleq a_{\mathrm{CT}}\ \delta(t-\tau_{\mathrm{CT}}), \tag{2}$$

$$h_{\mathrm{TR}}(t) \triangleq a_{\mathrm{TR}}\ \delta(t-\tau_{\mathrm{TR}}), \tag{3}$$

with $a_{\mathrm{CR}}, a_{\mathrm{CT}}, a_{\mathrm{TR}} \in \mathbb{R}$ the channel attenuation between carrier emitter and reader, carrier emitter and tag, tag and reader, respectively. The corresponding phases they introduce to the propagated signals are:

$$\phi_{\mathrm{CR}} \triangleq 2\pi F_c \tau_{\mathrm{CR}}, \tag{4}$$

$$\phi_{\mathrm{CT}} \triangleq 2\pi F_c \tau_{\mathrm{CT}}, \tag{5}$$

$$\phi_{\mathrm{TR}} \triangleq 2\pi F_c \tau_{\mathrm{TR}}, \tag{6}$$

where $\tau_{\mathrm{CR}}, \tau_{\mathrm{CT}}, \tau_{\mathrm{TR}}$ denote the signal propagation delay between carrier emitter and reader, carrier emitter and tag, tag and reader, respectively. The carrier emitter transmits a continuous wave of frequency F_c and power $P = A^2/2$:

$$c_{\mathrm{m}}(t) = A\cos(2\pi F_c t), \tag{7}$$

where the index "m" indicates that it is a real, passband signal. The RF tag receives from the carrier emitter:

$$c_{\mathrm{m}}(t) * h_{\mathrm{CT}}(t) = A\ a_{\mathrm{CT}}\cos(2\pi F_c(t-\tau_{\mathrm{CT}})) \tag{8}$$

$$= A\ a_{\mathrm{CT}}\cos(2\pi F_c t - \phi_{\mathrm{CT}}). \tag{9}$$

Modulation on the tag is achieved by switching its antenna load between multiple values which correspond to reflection coefficients $\Gamma_i, i = 0, \ldots, M-1$. The load reflection coefficient changes can be expressed as a function that takes M distinct values

$$\Gamma(t) \in \{\Gamma_i\}_{i=0}^{M-1}. \tag{10}$$

In this work, we consider two tag load values, and thus $\Gamma(t)$ may only take two values Γ_0, Γ_1. Recent work has exploited switching between M load values for higher-order modulation [22]. The tag complex baseband signal as a function of time is

$$x(t) \triangleq a_x(t)\ e^{j\phi_x(t)} = A_s - \Gamma(t), \tag{11}$$

where A_s is a load-independent term related to the antenna *structural mode* [13], [23]. It is noted that $\Gamma(t)$ and A_s are complex-valued. Then, the amplitude $a_x(t)$ is

$$a_x(t) \triangleq |A_s - \Gamma(t)|, \tag{12}$$

and the phase $\phi_x(t)$ is

$$\phi_x(t) \triangleq \angle(A_s - \Gamma(t)), \tag{13}$$

i.e. it is the angle of the complex quantity $A_s - \Gamma(t)$ in radians. The tag scatters back the signal

$$x_{\mathrm{m}}(t) = A\ a_{\mathrm{CT}}\ s(t)\ a_x(t)\cos(2\pi F_c t - \phi_{\mathrm{CT}} + \phi_x(t)), \tag{14}$$

where $s(t)$ is a scaling term related to the tag scattering efficiency and tag antenna gain at a given direction. The tag efficiency is generally considered time-varying, due to the use of rectifiers on passive tags. For a block of a few bits (e.g. one data packet), however, it may be considered constant. It can be also considered constant in the case of energy assisted (i.e. semipassive) tags where no incoming wave rectification takes place. From now on, we will be considering tag efficiency constant, and will thus simplify $s(t)$ to s.

The SDR receiver (reader) receives the superposition of the carrier emitter CW and the backscattered tag signal through channels $h_{\mathrm{CR}}(t)$ and $h_{\mathrm{TR}}(t)$, respectively:

$$y_m(t) = A\ [a_{\mathrm{CR}}\cos(2\pi F_c t - \phi_{\mathrm{CR}}) + a_{\mathrm{CT}}a_{\mathrm{TR}}s\ a_x(t-\tau_{\mathrm{TR}})\cos(2\pi F_c t - \phi_{\mathrm{CT}} - \phi_{\mathrm{TR}} + \phi_x(t-\tau_{\mathrm{TR}}))] + w(t), \tag{15}$$

where $w(t)$ is band-limited additive Gaussian noise with power spectral density (PSD)

$$S_w(F) = \begin{cases} \frac{N_0}{2}, & |F \pm F_c| \le W, \\ 0, & \text{elsewhere.} \end{cases} \tag{16}$$

$2W$ is the passband receiver bandwidth and $F_c >> W$. The reader demodulates the incoming signal with local oscillator (LO) carrier $F_c + \Delta F$ and phase ϕ_R, and then filters out the high frequency components. ΔF is the frequency difference between the emitter and the reader, i.e. it is the carrier frequency offset (CFO). The lowpass in-phase and quadrature components are:

$$I(t) = \mathtt{LPF}\{y_m(t)\cos(2\pi(F_c+\Delta F)t + \phi_R)\}, \tag{17}$$

$$Q(t) = \mathtt{LPF}\{-y_m(t)\sin(2\pi(F_c+\Delta F)t + \phi_R)\}. \tag{18}$$

After lowpass filtering around $[-W,\ W]$:

$$I(t) = \frac{Aa_{\mathrm{CR}}}{2}\cos(2\pi\Delta F t + \hat{\phi}_{\mathrm{CR}}) + \frac{sAa_{\mathrm{CT}}a_{\mathrm{TR}}}{2}a_x(t-\tau_{\mathrm{TR}})\cos(2\pi\Delta F t + \hat{\phi}_{\mathrm{CTR}} - \phi_x(t-\tau_{\mathrm{TR}})) + n_I(t), \tag{19}$$

$$Q(t) = -\frac{Aa_{\mathrm{CR}}}{2}\sin(2\pi\Delta F t + \hat{\phi}_{\mathrm{CR}}) - \frac{sAa_{\mathrm{CT}}a_{\mathrm{TR}}}{2}\ a_x(t-\tau_{\mathrm{TR}})\sin(2\pi\Delta F t + \hat{\phi}_{\mathrm{CTR}} - \phi_x(t-\tau_{\mathrm{TR}})) + n_Q(t), \tag{20}$$

with

$$\hat{\phi}_{\mathrm{CR}} \triangleq \phi_{\mathrm{CR}} + \phi_R, \tag{21}$$

$$\hat{\phi}_{\mathrm{CTR}} \triangleq \phi_{\mathrm{CT}} + \phi_{\mathrm{TR}} + \phi_R. \tag{22}$$

The terms $n_I(t), n_Q(t)$ are lowpass Gaussian noise components with PSD

$$S_{n_I}(F) = S_{n_Q}(F) = \begin{cases} \frac{N_0}{4}, & |F| \leq W, \\ 0, & \text{elsewhere}, \end{cases} \tag{23}$$

and variance

$$\sigma_n^2 = \mathbb{E}[n_I^2(t)] = \mathbb{E}[n_Q^2(t)] = \frac{N_0}{4} 2W = \frac{N_0 W}{2}. \tag{24}$$

The above can be derived using basic stochastic process theory [24]. The complex baseband signal is:

$$y(t) \triangleq I(t) + jQ(t) \tag{25}$$

$$= \frac{A}{2} \left[a_{\text{CR}}\ e^{-j\hat{\phi}_{\text{CR}}} + a_{\text{CT}} a_{\text{TR}} s\ x(t - \tau_{\text{TR}})\ e^{-j\hat{\phi}_{\text{CTR}}} \right] e^{-j2\pi\Delta F t} + n(t), \tag{26}$$

with $n(t) = n_I(t) + j n_Q(t)$ complex Gaussian noise, with zero-mean and variance $\mathbb{E}[|n(t)|^2] = \mathbb{E}[n_I^2(t)] + \mathbb{E}[n_Q^2(t)] = 2\sigma_n^2$.

Given the extended bit duration, it is assumed that wireless channels between the generator and the reader or the tag, as well as between the tag and the reader, change within a *small* number of consecutive bits, i.e. the channel coherence time spans a limited number of bits. On the contrary, for conventional high bit-rate applications, the channel coherence time spans a significantly larger number of bits. The same holds for the CFO, whose value has significantly changed within a limited number of bits.

III. Scatter Radio Link

For the bistatic scatter radio link, two modulation schemes are presented, each with its corresponding processing for sensor data decoding. The first one is based on on-off keying (OOK), which is a popular binary modulation scheme among commercial RFID systems. It is shown that even if a tag modulates information using binary phase shift keying (BPSK), or amplitude shift keying (ASK), or a hybrid of those two, it can be seen as an OOK modulation at the receiver side.[1] OOK is a modulation scheme suitable for the bandwidth-limited regime, while the second scheme presented is more suitable for the power-limited regime and is based on frequency shift keying (FSK). FSK modulation shows some advantages over OOK for backscatter networks, where extended range, simple multiple access, and increased receiver sensitivity are necessary. A complete comparison of the two schemes is given later in this work.

[1]For true BPSK, a semipassive tag has to switch between reflection coefficients $\Gamma_0 = 1$ and $\Gamma_1 = -1$. For ASK, the two reflection coefficients' amplitude values have to differ, but their phases shall remain the same, i.e. $|\Gamma_0| \neq |\Gamma_1|, \angle\Gamma_0 = \angle\Gamma_1$. For OOK, the tag has to switch between $\Gamma_0 = 0$ and $\Gamma_1 = 1$. In practice, most commercial tags perform a hybrid binary modulation scheme, since they switch between two arbitrary reflection coefficient values that may or may not keep the same amplitude or phase.

A. OOK

The antenna load's reflection coefficient is Γ_0 or Γ_1 for bit '0' or bit '1', respectively. Then the baseband scattered signal of Eq. (11) is expressed as:

$$x(t) = (A_s - \frac{\Gamma_0 + \Gamma_1}{2}) + \frac{\Gamma_0 - \Gamma_1}{2} \sum_{n=0}^{N-1} x_n\ \Pi(t - nT), \tag{27}$$

where $x_n \in \{-1, +1\}$ are the N transmitted bits and $\Pi(t)$ is a pulse of bit duration T:

$$\Pi(t) = \begin{cases} 1, & 0 \leq t < T, \\ 0, & \text{elsewhere}. \end{cases} \tag{28}$$

The scattered signal (27) can be written as:

$$x(t) = m_{\text{dc}}\ e^{j\theta_{\text{dc}}} + m_{\text{mod}}\ e^{j\theta_{\text{mod}}} \sum_{n=0}^{N-1} x_n\ \Pi(t - nT), \tag{29}$$

with

$$m_{\text{dc}} = |A_s - (\Gamma_0 + \Gamma_1)/2|,\ \theta_{\text{dc}} = \underline{\angle A_s - (\Gamma_0 + \Gamma_1)/2} \tag{30}$$

$$m_{\text{mod}} = |\Gamma_0 - \Gamma_1|/2,\ \theta_{\text{mod}} = \underline{\angle \Gamma_0 - \Gamma_1}. \tag{31}$$

The SDR receives according to (26) and (29):

$$y(t) = y_{\text{nl}}(t) + n(t) \tag{32}$$

$$= \left[\hat{m}_{\text{dc}} e^{j\hat{\phi}_{\text{dc}}} + \hat{m}_{\text{mod}} e^{j\hat{\phi}_{\text{mod}}} \sum_{n=0}^{N-1} x_n \Pi(t - \tau_{\text{TR}} - nT) \right] e^{-j2\pi\Delta F t} + n(t), \tag{33}$$

with

$$\hat{m}_{\text{dc}} e^{j\hat{\phi}_{\text{dc}}} \triangleq \frac{A}{2} \left[a_{\text{CR}} e^{-j\hat{\phi}_{\text{CR}}} + s a_{\text{CT}} a_{\text{TR}}\ m_{\text{dc}}\ e^{j(\theta_{\text{dc}} - \hat{\phi}_{\text{CTR}})} \right], \tag{34}$$

$$\hat{m}_{\text{mod}} e^{j\hat{\phi}_{\text{mod}}} \triangleq \frac{A}{2} s a_{\text{CT}} a_{\text{TR}}\ m_{\text{mod}}\ e^{j(\theta_{\text{mod}} - \hat{\phi}_{\text{CTR}})}. \tag{35}$$

After sampling the baseband signal with sampling period T_s, the digitized signal is given by:

$$y[k] = y(kT_s + \tau_{\text{TR}}) = y_{\text{nl}}[k] + n[k], \tag{36}$$

with $n[k] \sim \mathcal{CN}(0, 2\sigma_n^2)$.[2]

The term $y_{\text{nl}}[k]$ refers to the *noiseless* received signal that comprises of a DC component and a modulated component. The DC component comes from the combination of the CW received through the emitter-to-reader channel and an unmodulated component $m_{\text{dc}} e^{j\theta_{\text{dc}}}$ which is scattered by the tag. Notice that this noiseless received signal suffers from a CFO term, due to the oscillator inaccuracies on both the carrier emitter and the SDR reader. The CFO causes detector performance loss, and is thus strongly undesired. A way to eliminate the CFO term of the noiseless signal–without estimating it–is by taking the absolute value $|y_{\text{nl}}(t)|$. Then the receiver observes the *amplitude* of the received signal which takes two distinct

[2]Notation $n \sim \mathcal{CN}(0, 2\sigma^2)$ means that $n = n_r + j n_i$ is complex, circularly symmetric Gaussian, i.e. n_r, n_i are zero-mean, independent and identically distributed random variables according to Gaussian distribution $\mathcal{N}(0, \sigma^2)$.

values, according to the binary modulation performed by the tag. Specifically, the complex noiseless samples $y_{\text{nl}}[k]$ of the (carrier+tag) signal received have amplitude values which are denoted as:

$$s_k \triangleq |y_{\text{nl}}[k]| = \begin{cases} a, & \text{if bit '0'}, \\ b, & \text{if bit '1'}, \end{cases} \tag{37}$$

where, without loss of generality, it is assumed that $a < b$. In Fig. 3-upperleft, a backscattered OOK signal is shown as a function of time. Bit '0' is depicted as a low signal level a for duration T and bit '1' is shown as a high signal level b for duration T. Considering a as a reference level, it can be removed as an offset. This results in two levels, 0 and $b-a$, justifying the OOK terminology.

It is clear that the processing that will take place for the received tag signals is completely non-linear, since it depends on the nonlinear absolute operation. We will now define some useful quantities for the BER performance characterization of the proposed receivers. The carrier-to-noise ratio (CNR), is defined as:

$$\text{CNR} \triangleq \frac{a^2/2}{\mathbb{E}[|n[k]|^2]}\ L = \frac{a^2}{4\sigma^2}\ L, \tag{38}$$

where a^2 is the received carrier power (Fig. 3). The division of a^2 by 2 denotes that the carrier is an 'on-off' signal, i.e. the carrier generator may transmit a carrier wave, or not. $L \triangleq T/T_s$ is the oversampling factor, with T being the symbol duration (i.e. bit duration for binary modulation), and T_s being the sampling period. The CNR is an important quantity because, in sharp contrast to classic Marconi-type communicators which radiate their own carrier during transmission, the carrier in scatter radio is emitted from a different than the tag terminal. We define the tag signal-to-noise ratio (SNR), *after* the absolute operation, as:

$$\text{SNR} \triangleq \frac{(b-a)^2/2}{\mathbb{E}[|n[k]|^2]}\ L = \frac{(b-a)^2}{4\sigma^2}\ L. \tag{39}$$

Notice that the difference $b-a$ compared to noise power affects the success in detecting which bit was transmitted. Another useful quantity is introduced, namely the carrier-to-signal ratio (CSR),

$$\text{CSR} \triangleq \frac{\mathcal{P}_c}{\mathcal{P}_b} = \frac{a^2}{(b-a)^2}, \tag{40}$$

which indicates the ratio between the received carrier and the useful tag signal. Notice that $\text{CSR} = \text{CNR}/\text{SNR}$.

After squaring the absolute of the received signal, the result is:

$$|y[k]|^2 = |y_{\text{nl}}[k]|^2 + 2\Re\{y_{\text{nl}}[k]\ n^*[k]\} + |n[k]|^2. \tag{41}$$

The squared magnitude of the baseband signal $m_k^2 = |y[k]|^2$, for given $s_k \in \{a, b\}$, is the sum of two squared, independent Gaussians with the same variance and different means; thus, m_k^2 follows a non-central Chi-squared distribution with 2 degrees of freedom and non-centrality parameter s_k [25], which is independent of the CFO ΔF. Thus, the receiver can process m_k^2, without the need for estimating ΔF.

The squared magnitude $\{m_k^2\}$ of the received signal is filtered using a square pulse impulse response $\Pi[k]$, given by:

$$\Pi[k] = \begin{cases} 1, & 0 \le k \le L-1, \\ 0, & \text{otherwise}, \end{cases} \tag{42}$$

which has a length of L taps. The filtered signal is then sampled at the end of each symbol period and each sampled symbol is expressed as:

$$r \triangleq \sum_{k=0}^{L-1} m_k^2\ \Pi[L-1-k] = \sum_{k=0}^{L-1} |y[k]|^2. \tag{43}$$

Random variable r is the sum of L independent, identically distributed non-central Chi-squared random variables, and thus follows a non-central Chi-squared distribution with $2L$ degrees of freedom; its probability density function (PDF) is given by [26]:

$$f_R(r|s_R, 2L, \sigma_n^2) = \frac{1}{2\sigma_n^2}\left(\frac{r}{s_R^2}\right)^{\frac{L-1}{2}} \exp\left(-\frac{r+s_R^2}{2\sigma_n^2}\right) \times I_{L-1}\left(\frac{\sqrt{r}\ s_R}{\sigma_n^2}\right),\ r \ge 0, \tag{44}$$

where $I_v(\cdot)$ is the v-th order modified Bessel function of the first kind. The non-centrality parameter s_R is given by:

$$s_R^2 \triangleq \sum_{k=0}^{L-1} s_k^2 = \begin{cases} L\ a^2, & \text{if bit '0'}, \\ L\ b^2, & \text{if bit '1'}. \end{cases} \tag{45}$$

The cumulative distribution function (CDF) of random variable r is given by:

$$F_{R|s_R,2L,\sigma_n^2}(r) \triangleq \Pr(R \le r) = 1 - Q_L\left(\frac{s_R}{\sigma_n}, \frac{\sqrt{r}}{\sigma_n}\right), \tag{46}$$

where $Q_M(\lambda, \xi) = \int_\xi^\infty x\left(\frac{x}{\lambda}\right)^{M-1} \exp\left(-\frac{x^2+\lambda^2}{2}\right) I_{M-1}(\lambda x)\ dx$ is the generalized Marcum Q-function [27].

The minimum probability of error detector is needed for the following binary hypothesis problem:

$$\begin{aligned} H_0:&\ f_{R|H_0}(r|H_0) = f_R(r|s_a, 2L, \sigma_n^2), \quad s_a^2 = L\ a^2, \\ H_1:&\ f_{R|H_1}(r|H_1) = f_R(r|s_b, 2L, \sigma_n^2), \quad s_b^2 = L\ b^2. \end{aligned}$$

For equiprobable hypotheses, the minimum bit error rate (BER) detector is the maximum-likelihood (ML) detector, given by:

$$\begin{aligned} & f_{R|H_1}(r|H_1) \overset{H_1}{\ge} f_{R|H_0}(r|H_0) \\ \Leftrightarrow & \left(\frac{1}{s_b}\right)^{L-1} \exp\left(-\frac{r+s_b^2}{2\sigma_n^2}\right) I_{L-1}\left(\frac{\sqrt{r}\ s_b}{\sigma_n^2}\right) \\ & \overset{H_1}{\ge} \left(\frac{1}{s_a}\right)^{L-1} \exp\left(-\frac{r+s_a^2}{2\sigma_n^2}\right) I_{L-1}\left(\frac{\sqrt{r}\ s_a}{\sigma_n^2}\right). \end{aligned} \tag{47}$$

The above ML detector, even though BER-optimal, requires numerical computation of the two $L-1$-th order modified Bessel functions of the first kind. For large arguments of the

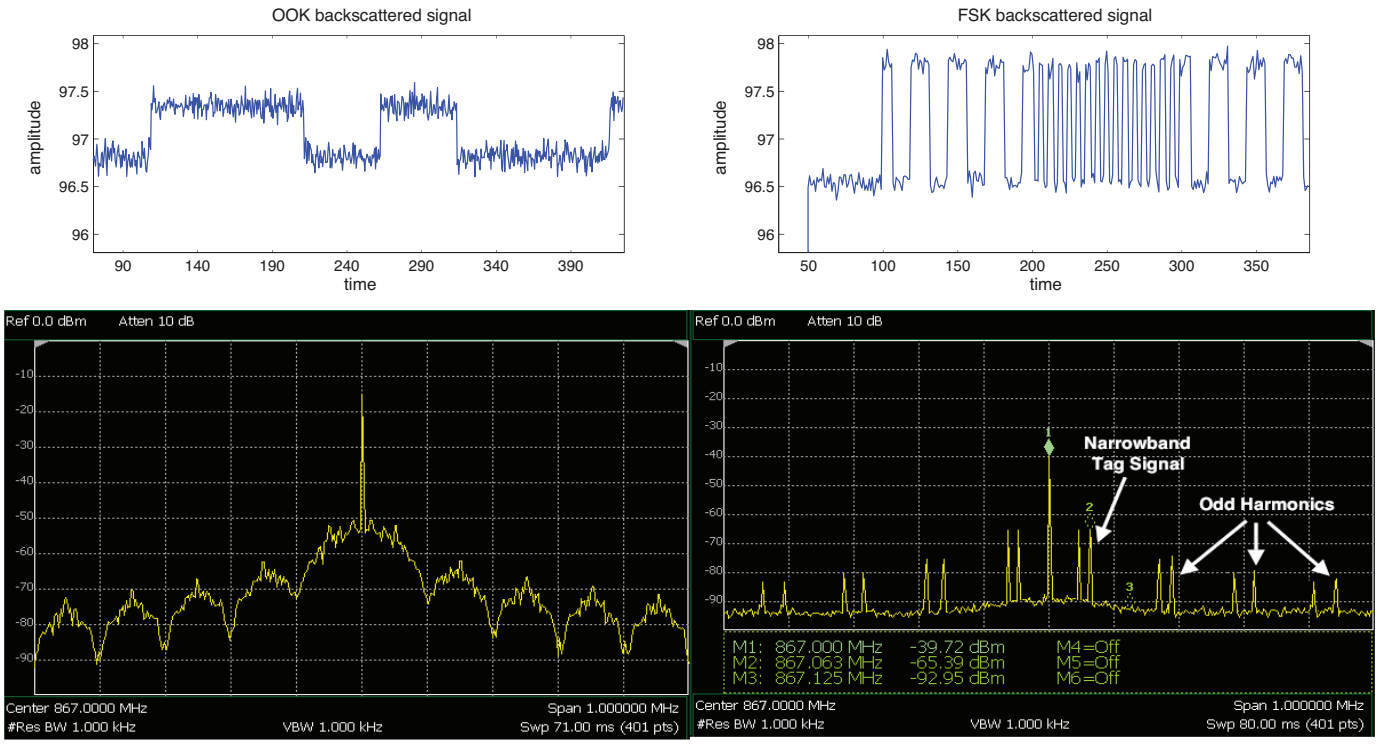

Fig. 3. Received signal from the experimental setup for the bandwidth-limited regime (OOK - left figures) and the power-limited regime (FSK - right figures). Both time (top) and frequency (bottom) domain plots are provided.

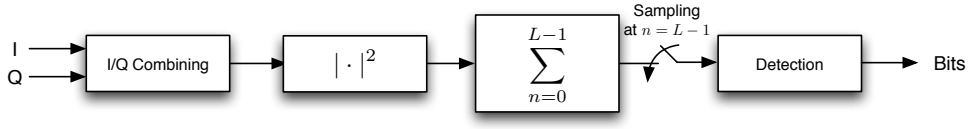

Fig. 4. Signal processing chain for OOK backscattered data.

functions $I_{L-1}(\cdot)$, the approximation $I_{L-1}(z) \approx \frac{\exp(z)}{\sqrt{2\pi z}}$ [27] simplifies the above detector to:

$$\exp\left(\frac{s_a^2 - s_b^2}{2\sigma_n^2}\right) \frac{\exp\left(\frac{\sqrt{r}\ s_b}{\sigma_n^2}\right)}{\sqrt{2\pi \frac{\sqrt{r}\ s_b}{\sigma_n^2}}} \underset{H_0}{\overset{H_1}{\geq}} \left(\frac{s_b}{s_a}\right)^{L-1} \frac{\exp\left(\frac{\sqrt{r}\ s_a}{\sigma_n^2}\right)}{\sqrt{2\pi \frac{\sqrt{r}\ s_a}{\sigma_n^2}}}$$

$$\Leftrightarrow r \underset{H_0}{\overset{H_1}{\geq}} \left[\frac{\sigma_n^2}{s_b - s_a}(L - \frac{1}{2}) \ln(s_b/s_a) + \frac{s_b + s_a}{2}\right]^2 \triangleq \eta_1, \quad (48)$$

where we have taken $s_b > s_a$ into account. The above detector requires estimation of the parameters a, b, σ_n^2. It will be shown in the numerical results that the BER performance of the above detector coincides with the ML detector performance for high CSR values, which is the typical case in scatter radio.

A simple (heuristic) detector is also tested, in order to bypass the need for Bessel function computation as well as the need for estimation of parameters a, b, σ^2. This appealing detector calculates the average value of a received preamble, other than the information data, and utilizes such value as the decision threshold. The heuristic detector is given by:

$$r \underset{H_0}{\overset{H_1}{\geq}} \frac{1}{N_p} \sum_{i=0}^{N_p - 1} \tilde{r}_i \triangleq \eta_2, \quad (49)$$

where $\tilde{r}_i,\ i = 0, \ldots, N_p - 1$ are the N_p preamble symbols (which are independent of the data) after filtering with $\Pi[k]$ and sampling. The above heuristic detector requires the calculation of the above threshold only, and no further estimation of the parameters a, b, σ^2. Notice however, that the number N_p cannot be made arbitrarily large, since in that case the channel values (and hence parameters a, b) may have changed.

The above processing, summarized in Fig. 4, as well as the described detectors, assume symbol synchronization, which can be implemented using correlation with a sequence of known bits in the preamble. Moreover, the receiver needs to determine whether the information bits have been flipped due to channel conditions (i.e. high level has become low and vice versa). This is managed through comparison of the detected preamble bits with the a priori known bit sequence.

B. FSK

In FSK, the tag switches between two distinct reflection coefficient values Γ_0, Γ_1 with different rates F_i for corresponding bits $i = 0, 1$ (also called subcarrier frequencies). To ensure orthogonality in noncoherent FSK, the spacing between the two subcarrier frequencies is $|F_1 - F_0| = k\frac{1}{T},\ k \in \mathbb{N}$, where T is the bit duration. For N bits $x_n \in \{0, 1\}$, the baseband

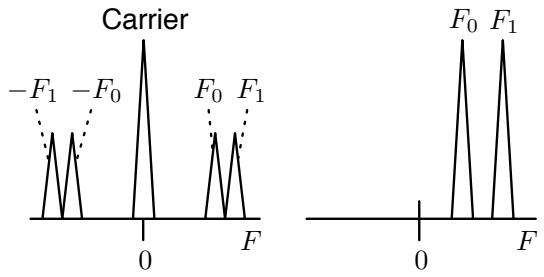

Fig. 5. Complex baseband spectrum for backscatter FSK (left) and 'classic' FSK (right). Two subcarriers per frequency exist in backscatter FSK, in contrast with classic FSK.

scattered FSK waveform can be written as

$$x(t) = (A_s - \frac{\Gamma_0 + \Gamma_1}{2}) + \frac{\Gamma_0 - \Gamma_1}{2} \sum_{n=0}^{N-1} b(x_n, t - nT), \tag{50}$$

where $b(i,t)$ represents a 50% duty cycle square waveform of frequency F_i, random initial phase $\Phi \sim \mathcal{U}[0, 2\pi)$, amplitude 1 (i.e. level switches between -1 and $+1$), and duration T:

$$b(i,t) = \begin{cases} \frac{4}{\pi} \sum_{k=0}^{+\infty} \frac{1}{2k+1} \cos[(2k+1)(2\pi F_i t + \Phi)], & 0 \le t < T, \\ 0, & \text{elsewhere.} \end{cases} \tag{51}$$

Because of the limited receiver bandwidth, we consider that $3F_i >> W$. Keeping only the fundamental frequency component of $b(i,t)$ and substituting it in (50), the (filtered) tag complex baseband scattered waveform for *one* bit duration is written as

$$\tilde{x}(t) = (A_s - \frac{\Gamma_0 + \Gamma_1}{2}) + \frac{\Gamma_0 - \Gamma_1}{2} \frac{4}{\pi} \cos(2\pi F_i t + \Phi) \tag{52}$$

$$= m_{\text{dc}}\ e^{j\theta_{\text{dc}}} + m_{\text{mod}} \cos(2\pi F_i t + \Phi)\ e^{j\theta_{\text{mod}}}, \tag{53}$$

with

$$m_{\text{dc}} = |A_s - (\Gamma_0 + \Gamma_1)/2|,\ \theta_{\text{dc}} = \underline{\angle A_s - (\Gamma_0 + \Gamma_1)/2} \tag{54}$$

$$m_{\text{mod}} = 2|\Gamma_0 - \Gamma_1|/\pi,\ \theta_{\text{mod}} = \underline{\angle \Gamma_0 - \Gamma_1}. \tag{55}$$

According to Eq. (26), the SDR receives:

$$y(t) = \left[\hat{m}_{\text{dc}}\ e^{j\hat{\phi}_{\text{dc}}} + \hat{m}_{\text{mod}} \cos(2\pi F_i t + \Phi')\ e^{j\hat{\phi}_{\text{mod}}}\right] e^{-j2\pi\Delta F t} + n(t), \tag{56}$$

with

$$\hat{m}_{\text{dc}} e^{j\hat{\phi}_{\text{dc}}} \triangleq \frac{A}{2} [a_{\text{CR}} e^{-j\hat{\phi}_{\text{CR}}} + s a_{\text{CT}} a_{\text{TR}}\ m_{\text{dc}}\ e^{j(\theta_{\text{dc}} - \hat{\phi}_{\text{CTR}})}], \tag{57}$$

$$\hat{m}_{\text{mod}} e^{j\hat{\phi}_{\text{mod}}} \triangleq \frac{A}{2} s a_{\text{CT}} a_{\text{TR}}\ m_{\text{mod}}\ e^{j(\theta_{\text{mod}} - \hat{\phi}_{\text{CTR}})}, \tag{58}$$

$$\Phi' \triangleq \Phi - 2\pi F_i \tau_{\text{TR}}. \tag{59}$$

In Fig. 5 the spectrum of the complex baseband is shown, for scatter radio FSK and for 'classic' FSK. Notice that because of the scatter radio tag modulation directly at passband, *two* subcarriers appear for each frequency F_i, one at the positive semiaxis and one at the negative (Fig. 5-left). In contrast, for a classic active FSK transmitter, only one subcarrier appears for each frequency (Fig. 5-right). For the latter, an FSK receiver is used which correlates against frequencies F_0 and F_1 for signal demodulation [28]. However, if the same receiver is applied for scatter radio FSK, only the subcarriers at frequencies F_0 and F_1 will be considered, leaving out $-F_0$ and $-F_1$. This results in a 3dB loss of information and degraded receiver performance. The above show that a classic FSK receiver is not applicable in scatter radio, since it does not account for the correct signal model of the scatter radio link. Thus, a different processing chain has to be designed for successful signal demodulation.

Assuming no CFO (i.e. $\Delta F = 0$), the received waveform is

$$y(t) = \hat{m}_{\text{dc}}\ e^{j\hat{\phi}_{\text{dc}}} + \hat{m}_{\text{mod}} \cos(2\pi F_i t + \Phi')\ e^{j\hat{\phi}_{\text{mod}}} + n(t). \tag{60}$$

After sampling with sampling period T_s, the baseband digitized signal is

$$y[k] = y(kT_s)$$

$$= \hat{m}_{\text{dc}}\ e^{j\hat{\phi}_{\text{dc}}} + \hat{m}_{\text{mod}} \cos(2\pi F_i k T_s + \Phi')\ e^{j\hat{\phi}_3} + n[k], \tag{61}$$

with $n[k] \sim \mathcal{CN}(0, 2\sigma_n^2)$. The DC term $\hat{m}_{\text{dc}}\ e^{j\hat{\phi}_{\text{dc}}}$ does not contribute any information on the transmitted data, and so it can be blocked using a DC-blocking filter.[3] After DC-blocking, the waveform is

$$\tilde{y}[k] = \hat{m}_{\text{mod}} \cos(2\pi F_i k T_s + \Phi')\ e^{j\hat{\phi}_3} + n[k]. \tag{62}$$

The received SNR at baseband is

$$\text{SNR} \triangleq \frac{\hat{m}_{\text{mod}}^2/2}{\mathbb{E}[|n[k]|^2]}\ L = \frac{\hat{m}_{\text{mod}}^2}{4\sigma_n^2}\ L. \tag{63}$$

Observing (62), we can notice that a 'classic' non-coherent FSK demodulator (envelope detector) cannot be directly applied for demodulating the received signal, due to the presence of the unknown term $e^{j\hat{\phi}_{\text{mod}}}$. Equation (62) can be rewritten as

$$\tilde{y}[k] = \frac{\hat{m}_{\text{mod}}}{2} e^{j(2\pi F_i k T_s + \Phi' + \hat{\phi}_3)} + \frac{\hat{m}_{\text{mod}}}{2} e^{-j(2\pi F_i k T_s + \Phi' - \hat{\phi}_3)} + n[k]. \tag{64}$$

Thus the received signal is a sum of two complex exponentials, of frequencies F_i and $-F_i$, respectively, and unknown phases $(\Phi' + \hat{\phi}_{\text{mod}})$ and $(-\Phi' + \hat{\phi}_{\text{mod}})$. Any two exponentials with frequencies $\pm F_0, \pm F_1$ are orthogonal ([24]), and a correlation demodulator that exploits the orthogonality can be used for demodulation. For one bit duration T, a bank of correlation demodulators processes $L = T/T_s$ samples and yields the

[3]DC-blocking can be implemented by estimation and removal of the received signal's mean value $\mathcal{E}\{y(t)\}$.

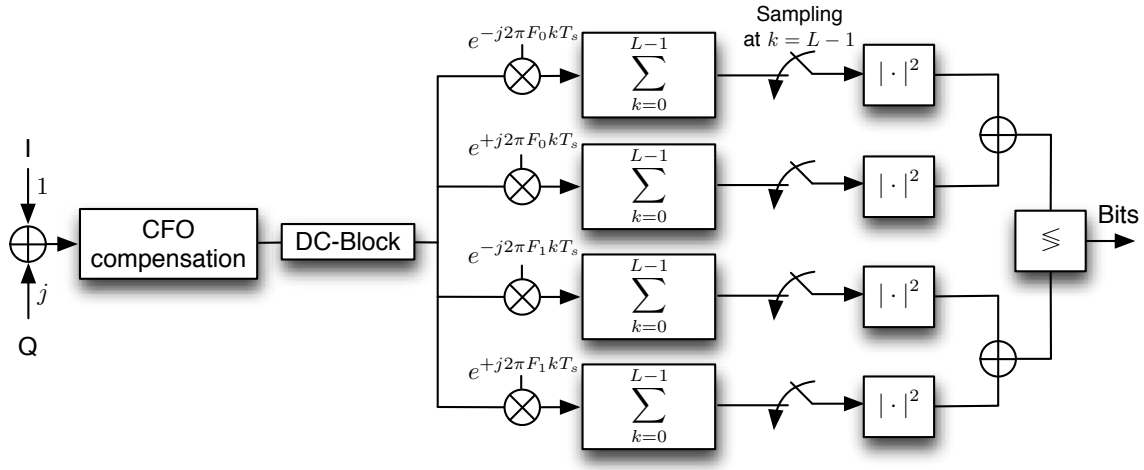

Fig. 6. Backscatter FSK signal processing chain. After CFO compensation and DC-blocking, the complex baseband signal is correlated against $\pm F_0, \pm F_1$ for L samples, which correspond to one bit duration T. Then, the correlator outputs are sampled and detection is performed on the samples.

statistics

$$r_0^+ = \sum_{k=0}^{L-1} \tilde{y}[k]\ e^{-j2\pi F_0 kT_s} \tag{65}$$

$$= \frac{\hat{m}_{\text{mod}}}{2} \sum_{k=0}^{L-1} e^{j(2\pi(F_i-F_0)kT_s+\Phi'+\hat{\phi}_{\text{mod}})} + \underbrace{\frac{\hat{m}_{\text{mod}}}{2} \sum_{k=0}^{L-1} e^{-j(2\pi(F_i+F_0)kT_s+\Phi'-\hat{\phi}_{\text{mod}})}}_{\approx 0} + \sum_{k=0}^{L-1} n'[k]$$

$$= \frac{\hat{m}_{\text{mod}}}{2} \sum_{k=0}^{L-1} e^{+j(2\pi(F_i-F_0)kT_s+\Phi'+\hat{\phi}_{\text{mod}})} + n_0^+. \tag{66}$$

Notice that the sum of the "fast" exponential with frequency $F_i + F_0$ is approximated by zero. Also, notice that the noise term $n'[k] \triangleq n[k]\ e^{\pm j2\pi F_i kT_s}$ follows the same distribution with $n[k]$, i.e. it is circularly-symmetric Gaussian. The other correlator statistics are:

$$r_0^- = \sum_{k=0}^{L-1} \tilde{y}[k]\ e^{+j2\pi F_0 kT_s}$$

$$= \frac{\hat{m}_{\text{mod}}}{2} \sum_{k=0}^{L-1} e^{-j(2\pi(F_i-F_0)kT_s+\Phi'-\hat{\phi}_{\text{mod}})} + n_0^- \tag{67}$$

$$r_1^+ = \sum_{k=0}^{L-1} \tilde{y}[k]\ e^{-j2\pi F_1 kT_s}$$

$$= \frac{\hat{m}_{\text{mod}}}{2} \sum_{k=0}^{L-1} e^{+j(2\pi(F_i-F_1)kT_s+\Phi'+\hat{\phi}_{\text{mod}})} + n_1^+ \tag{68}$$

$$r_1^- = \sum_{k=0}^{L-1} \tilde{y}[k]\ e^{+j2\pi F_1 kT_s}$$

$$= \frac{\hat{m}_{\text{mod}}}{2} \sum_{k=0}^{L-1} e^{-j(2\pi(F_i-F_1)kT_s+\Phi'-\hat{\phi}_{\text{mod}})} + n_1^- \tag{69}$$

When bit '1' is transmitted, the received signal has frequency F_1 and thus, the statistics are

$$r_0^+ = n_0^+, \qquad r_1^+ = \frac{\hat{m}_{\text{mod}}\ L}{2}\ e^{+j(\Phi'+\hat{\phi}_{\text{mod}})} + n_1^+ \tag{70}$$

$$r_0^- = n_0^-, \qquad r_1^- = \frac{\hat{m}_{\text{mod}}\ L}{2}\ e^{-j(\Phi'-\hat{\phi}_{\text{mod}})} + n_1^- \tag{71}$$

On the contrary, when bit '0' is transmitted, the received signal has frequency F_0 and thus, the statistics are

$$r_0^+ = \frac{\hat{m}_{\text{mod}}\ L}{2}\ e^{+j(\Phi'+\hat{\phi}_{\text{mod}})} + n_0^+, \qquad r_1^+ = n_1^+ \tag{72}$$

$$r_0^- = \frac{\hat{m}_{\text{mod}}\ L}{2}\ e^{-j(\Phi'-\hat{\phi}_{\text{mod}})} + n_0^-, \qquad r_1^- = n_1^- \tag{73}$$

Exploiting the statistics at the output of the demodulator, we make use of the detector

$$z_1 \triangleq |r_1^+|^2 + |r_1^-|^2 \overset{H_1}{\geq} |r_0^+|^2 + |r_0^-|^2 \triangleq z_0. \tag{74}$$

C. CFO Compensation for FSK Receiver

Consider (56) with a non-zero CFO ΔF. Then $y(t)$ will be a signal of frequency $\pm F_0 + \Delta F$ or $\pm F_1 + \Delta_F$; thus it can not be directly correlated against the frequencies $\pm F_0$ and $\pm F_1$. The CFO has to be compensated for successful demodulation and detection. For a *limited* number of bits, where the CFO may be considered static, a per-packet CFO estimation can be achieved using fast fourier transform (FFT) techniques. The periodogram of each packet is calculated with a high frequency resolution $dF \triangleq F_s/N_F$, where N_F is the number of FFT points, such that $dF << 1/T$. The CFO is estimated by finding the periodogram peak (which corresponds to the transmitted carrier), and is cancelled out by shifting the periodogram to DC. It is noted that for ultra low-bitrate scenarios where T is maximized, N_F has to be large for achieving a high frequency resolution. This requires a long processing time, which may be prohibiting in some scenarios. In the case that longer tag transmissions are required (i.e. in applications with long data sequences), the CFO may change within a packet, and thus the periodogram-based estimation is not a valid option. In such cases, a frequency tracking

loop should be utilized, to constantly track carrier changes and remove the unwanted CFO term.

IV. BER Performance

A. OOK

BER calculation for the approximate, high-CSR detector of Eq. (48) is given by:

$$\begin{aligned}\Pr(e_{\text{approx}}) &= \frac{1}{2}\Pr(e|H_1) + \frac{1}{2}\Pr(e|H_0)\\ &= \frac{1}{2}\Pr(R<\eta_1|H_1) + \frac{1}{2}\Pr(R\geq\eta_1|H_0)\\ &= \frac{1}{2}F_{R|s_b,2L,\sigma_n^2}(\eta_1) + \frac{1}{2}(1-F_{R|s_a,2L,\sigma_n^2}(\eta_1))\\ &= \frac{1}{2} - \frac{1}{2}Q_L\left(\frac{s_b}{\sigma_n},\frac{\sqrt{\eta_1}}{\sigma_n}\right) + \frac{1}{2}Q_L\left(\frac{s_a}{\sigma_n},\frac{\sqrt{\eta_1}}{\sigma_n}\right).\end{aligned} \tag{75}$$

Similarly, BER for the heuristic detector is given by:

$$\Pr(e_{\text{heuristic}}) = \frac{1}{2}\Pr(R<\eta_2|H_1) + \frac{1}{2}\Pr(R\geq\eta_2|H_0). \tag{76}$$

Notice that η_2 is preamble-dependent, and therefore, is a random threshold. When the threshold is based on N equiprobable '0's and '1's, it can be written in the following form:

$$\eta_2 = \sum_{i=0}^{N_p/2-1}\sum_{l=0}^{L-1}(X_{I,i,l}^2 + X_{Q,i,l}^2) + \sum_{i=N_p/2}^{N_p-1}\sum_{l=0}^{L-1}(X_{I,i,l}^2 + X_{Q,i,l}^2), \tag{77}$$

with

$$\begin{aligned}X_{I,i,l} &\sim \mathcal{N}\left(\frac{\Re\{y_a\}}{\sqrt{N_p}},\frac{\sigma_n^2}{N_p}\right),\ i=0,\ldots,N_p/2-1,\forall\ l,\\ X_{I,i,l} &\sim \mathcal{N}\left(\frac{\Re\{y_b\}}{\sqrt{N_p}},\frac{\sigma_n^2}{N_p}\right),\ i=N_p/2,\ldots,N_p-1,\forall\ l,\\ X_{Q,i,l} &\sim \mathcal{N}\left(\frac{\Im\{y_a\}}{\sqrt{N_p}},\frac{\sigma_n^2}{N_p}\right),\ i=0,\ldots,N_p/2-1,\forall\ l,\\ X_{Q,i,l} &\sim \mathcal{N}\left(\frac{\Im\{y_b\}}{\sqrt{N_p}},\frac{\sigma_n^2}{N_p}\right),\ i=N_p/2,\ldots,N_p-1,\forall\ l.\end{aligned}$$

$\mathcal{N}(\mu_i,\sigma_i^2)$ denotes the (real) normal pdf, with (real) mean μ_i and variance σ_i^2 and y_a, y_b denote the values of y_{nl} when bit '0' or bit '1' is transmitted, respectively. The above also assume that N_p is an even number. Then, η_2 follows the non-central Chi-squared distribution with $2N_pL$ degrees of freedom and non-centrality parameter s_{η_2} given by:

$$s_{\eta_2}^2 = L\ \frac{a^2+b^2}{2}, \tag{78}$$

which is independent of N_p. Thus, the pdf of η_2 is given by:

$$\begin{aligned}f_{\eta_2}(\eta_2|s_{\eta_2},2NL,\sigma_{\eta_2}^2) &= \frac{1}{2\sigma_{\eta_2}^2}\left(\frac{\eta_2}{s_{\eta_2}^2}\right)^{\frac{NL-1}{2}}\exp\left(-\frac{\eta_2+s_{\eta_2}^2}{2\sigma_{\eta_2}^2}\right)\\ &\times I_{N_pL-1}\left(\frac{\sqrt{\eta_2}\ s_{\eta_2}}{\sigma_{\eta_2}^2}\right),\ \eta_2\geq 0,\end{aligned} \tag{79}$$

where $\sigma_{\eta_2}^2 = \sigma_n^2/N_p$. We can now calculate the probabilities $\Pr(R<\eta_2|H_1)$ and $\Pr(R\geq\eta_2|H_0)$ using the law of iterated expectation:

$$\begin{aligned}\Pr(R<\eta_2|H_1) &= \mathop{\mathbb{E}}_{\eta_2}[\Pr(R<\eta_2|H_1,\eta_2)]\\ &= 1-\int_0^\infty Q_L\left(\frac{s_b}{\sigma_n},\frac{\sqrt{\eta_2}}{\sigma_n}\right)\ f_{\eta_2}(\eta_2|s_{\eta_2},2N_pL,\sigma_{\eta_2}^2)\ d\eta_2.\end{aligned} \tag{80}$$

Similarly,

$$\begin{aligned}\Pr(R\geq\eta_2|H_0) &= \mathop{\mathbb{E}}_{\eta_2}[\Pr(R>\eta_2|H_0,\eta_2)]\\ &= \int_0^\infty Q_L\left(\frac{s_a}{\sigma_n},\frac{\sqrt{\eta_2}}{\sigma_n}\right)\ f_{\eta_2}(\eta_2|s_{\eta_2},2N_pL,\sigma_{\eta_2}^2)\ d\eta_2.\end{aligned} \tag{81}$$

Substituting the two above terms in (76), the BER of the heuristic detector becomes:

$$\begin{aligned}&\Pr(e_{\text{heuristic}})\\ &= \frac{1}{2} - \frac{1}{2}\mathop{\mathbb{E}}_{\eta_2}\left[Q_L\left(\frac{s_b}{\sigma_n},\frac{\sqrt{\eta_2}}{\sigma_n}\right) - Q_L\left(\frac{s_a}{\sigma_n},\frac{\sqrt{\eta_2}}{\sigma_n}\right)\right].\end{aligned} \tag{82}$$

B. FSK

Under H_1 (bit '1' transmitted) the statistics at the correlator outputs are distributed as shown below [24]:

$$r_0^+ \sim \mathcal{CN}(0,2\sigma_n^2\ L), \tag{83}$$

$$r_0^- \sim \mathcal{CN}(0,2\sigma_n^2\ L), \tag{84}$$

$$r_1^+ \sim \mathcal{CN}(\frac{\hat{m}_{\text{mod}}\ L}{2}\ e^{-j(\Phi'-\hat{\phi}_{\text{mod}})},2\sigma_n^2\ L), \tag{85}$$

$$r_1^- \sim \mathcal{CN}(\frac{\hat{m}_{\text{mod}}\ L}{2}\ e^{-j(\Phi'-\hat{\phi}_{\text{mod}})},2\sigma_n^2\ L). \tag{86}$$

Then $z_0 = |r_0^+|^2 + |r_0^-|^2$ is the sum of 4 squared zero-mean Gaussian random variables, each with variance $\sigma^2 = \sigma_n^2\ L$. Thus z_0 follows a Chi-squared distribution with 4 degrees of freedom [26]:

$$f_{z_0}(z_0|\sigma^2,H_1) = \frac{z_0}{4\sigma^4}\exp\left\{-\frac{z_0}{2\sigma^2}\right\},\ z_0\geq 0 \tag{87}$$

$$F_{z_0}(z_0|\sigma^2,H_1) = 1-\exp\left\{-\frac{z_0}{2\sigma^2}\right\}\left(1+\frac{z_0}{2\sigma^2}\right). \tag{88}$$

The random variable $z_1 = |r_1^+|^2 + |r_1^-|^2$ is the sum of 4 squared non-zero-mean Gaussian random variables, each with variance $\sigma^2 = \sigma_n^2\ L$. Then z_1 follows a non-central Chi-squared distribution with 4 degrees of freedom. We determine the non-centrality parameter s^2 as follows:

$$\begin{aligned}s^2 &= \left|\frac{\hat{m}_{\text{mod}}\ L}{2}\ e^{+j(\Phi'+\hat{\phi}_{\text{mod}})}\right|^2 + \left|\frac{\hat{m}_{\text{mod}}\ L}{2}\ e^{-j(\Phi'-\hat{\phi}_{\text{mod}})}\right|^2\\ &= \frac{\hat{m}_{\text{mod}}^2\ L^2}{2}.\end{aligned} \tag{89}$$

The PDF and CDF of z_1 are:

$$f_{z_1}(z_1|s^2,\sigma^2,H_1) = \frac{\sqrt{z_1}}{2\sigma^2 s}\exp\left\{-\frac{z_1+s^2}{2\sigma^2}\right\}I_1\left(\sqrt{z_1}\frac{s}{\sigma^2}\right), \tag{90}$$

$$F_{z_1}(z_1|s^2,\sigma^2,H_1) = 1-Q_2\left(\frac{s}{\sigma},\frac{\sqrt{z_1}}{\sigma}\right),\ z_1\geq 0. \tag{91}$$

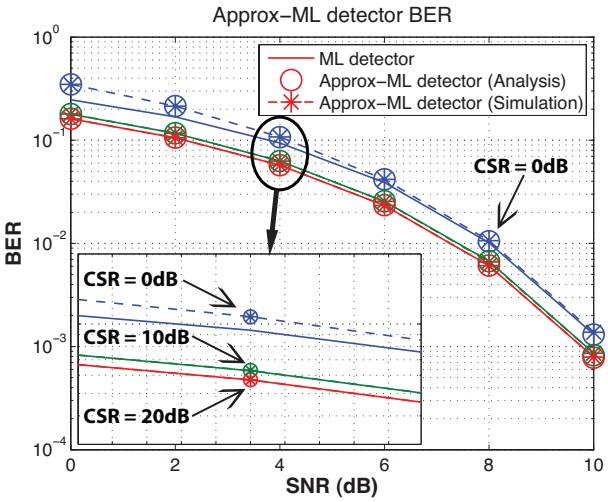

Fig. 7. Bit error rate for ML and the approx-ML detector, with $L = 10$.

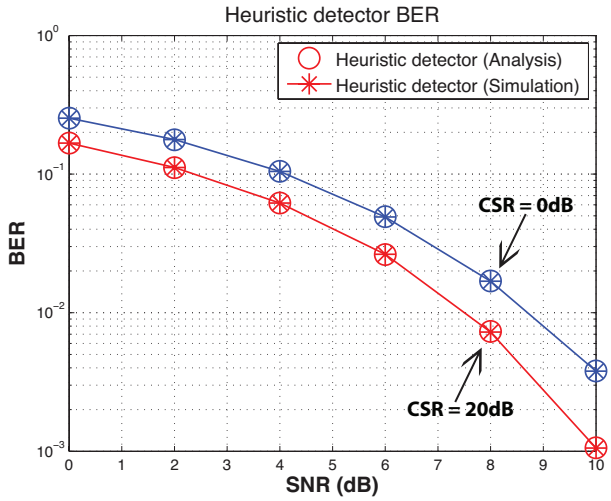

Fig. 8. Bit error rate of the heuristic detector, with $L = 10$.

The probability of correct decision under H_1 is

$$\Pr(c|H_1) = \Pr(z_0 \leq z_1|H_1) = \tag{92}$$

$$= \mathop{\mathbb{E}}_{z_1}[\Pr(z_0 \leq z_1|z_1, H_1)] = \mathop{\mathbb{E}}_{z_1}[F_{z_0|H_1}(z_1|H_1)]$$

$$= \int_0^\infty F_{z_0|H_1}(z_1|H_1)\ f_{z_1|H_1}(z_1|s^2, \sigma^2, H_1)\ dz_1 \tag{93}$$

Then the probability of error is

$$\Pr(e) = \Pr(e|H_0) = \Pr(e|H_1) = 1 - \Pr(c|H_1). \tag{94}$$

V. Numerical Results

A. OOK

Fig. 7 shows the performance of the approximate-ML detector of Eq. (48). SNR and CSR quantities follow the definitions of Section III-A. It can be seen that analysis matches simulation results. More importantly, for large SNR values the performance of the approximate detector coincides with the performance of the optimal ML detector, even for low CSR value of 0 dB. For higher CSR values, on the order of 10 dB, the performance gap between the two detectors is reduced, even for low SNR values. This is important, since, in practical setups, the calculation of the respective Bessel function may not be practical. Thus, it is concluded that the approximate detector of Eq. (48) is near-optimal. It is also seen that for a given SNR value, the increase in CSR (and thus in CNR also) improves BER performance for the particular detector.

That is an interesting result which directs optimization of the carrier power scattered from the tag towards the receiver and it is in sharp contrast to conventional tag design principles applied so far, that aim to optimize SNR only. Thus, tag design should aim to maximize not only SNR but also CNR (or CSR), for the proposed detector. Notice however, that performance for CSR values over 20dB is not significantly improved (as opposed to CSR values between 0 and 10 dB).

Fig. 8 depicts the BER performance of the heuristic detector with analytic as well as simulation results, which perfectly match. It is shown that a higher CSR value of 20 dB improves performance, compared to CSR of 0 dB, for the same reasons

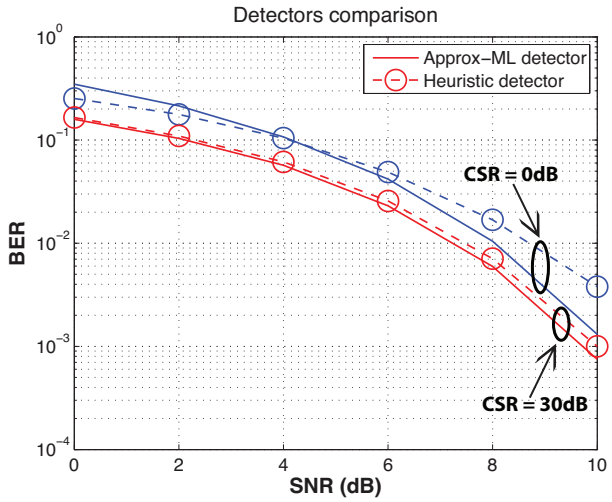

Fig. 9. Comparison of approx-ML and heuristic detectors.

as in the approx-ML detector. It is re-affirmed that tag design should not only maximize SNR values (namely the difference $b - a$) but also CNR (the values a, b, and respectively the CSR), when receiving architectures of this work are planned. Practical ways to design tags that adhere to the above design rules (both SNR and CNR maximization) can be found in [13].

Fig. 9 compares the near-optimal, approximate ML detector with the heuristic detector, based on their BER performance. It can be seen that for larger values of the CSR, the heuristic detector approaches the performance of the near-optimal, with a performance penalty of less than 0.5 dB. The advantage of the heuristic detector is its simple threshold calculation, which does not require knowledge of the noise variance or the values a, b, and can be acquired using a series of pilot symbols, provided that the channel will not change during the detection (i.e. the threshold will be estimated on preamble bits and utilized on data under the same channel conditions).

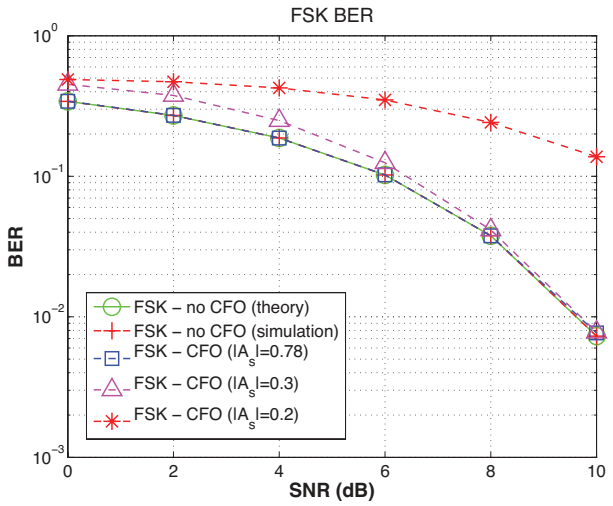

Fig. 10. Bit error probability as a function of SNR for backscatter FSK, for no CFO and compensated CFO scenarios with $a_{\text{CR}} = 0$.

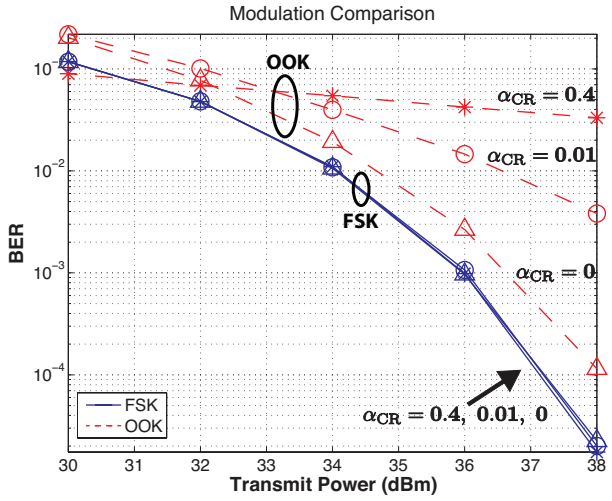

Fig. 11. Modulation comparison for the bistatic backscatter link. FSK and OOK compared in terms of BER as a function of the emitter transmit power and the emitter-to-reader channel factor a_{CR}.

B. FSK

The probability of error for backscatter FSK is shown in Fig. 10. The SNR follows the definition of Section III-B. Analysis BER of Eq. (94) perfectly matches with simulation, with no CFO between the carrier emitter and the receiver. Next, we characterize the performance of the FSK receiver in the presence of CFO. According to Section III-C, a strong DC term has to be received for successful CFO estimation (Eq. (54)). In most scenarios, a strong carrier will be available at the receiver from the emitter-to-reader path (Fig. 2), and thus carrier recovery will be successful. However, in the case of emitter-to-reader path blockage (i.e. $a_{\text{CR}} = 0$), no DC component from the emitter will be available at the reader. Then the only factor that will contribute a DC to the reader will be the unmodulated carrier reflected by the tag due to the antenna *structural* mode.

To minimize BER, the condition $|\Gamma_0 - \Gamma_1| = 2$ must hold for semipassive tags, as stated in [13]. Without loss of generality, the values $\Gamma_0 = 1$ and $\Gamma_1 = -1$ are chosen for the simulations. Recall from Eq. (54) that the backscattered DC amplitude is $|A_s - (\Gamma_0 + \Gamma_1)/2|$. For the *specific* value pair of reflection coefficients, the DC will relate directly to $|A_s|$, which will determine the backscattered carrier power. To show the necessity of tag design with respect to A_s, several values of A_s are tested; the values are $A_s = 0.6047 + j0.5042$ with $|A_s| \approx 0.78$, $A_s = 0.2954 - j0.0524$ with $|A_s| = 0.3$, and $A_s = 0.1593 - j0.1209$ with $|A_s| = 0.2$. It can be seen that as $|A_s|$ grows, the BER drops faster and approaches the theoretical curve, due to higher CFO estimation accuracy (due to stronger scattered carrier). This essentially suggests that the antenna structural mode is an important parameter to look after during tag design *along* with the pair of Γ_0, Γ_1 values. For the proposed FSK receiver, the tag designer should try to maximize $|A_s - (\Gamma_0 + \Gamma_1)/2|$. This could be achieved by either choosing appropriate Γ-values for a given A_s value, or by designing an antenna with an appropriate A_s value for a given pair of Γ_0, Γ_1. In either case, it is directed that antenna parameters and antenna load values should be taken *jointly* into account to maximize the receiver's BER performance.

C. Modulation Comparison

The two modulation schemes are compared in terms of BER performance in Fig. 11. The carrier emitter power (in dBm) is used as reference, since the SNR definitions differ for OOK and FSK, according to Eq. (39) and Eq. (63). The noise variance is the same for both modulation schemes. For OOK, the approximate-ML detector is used, and for FSK the periodogram-based CFO compensation technique is chosen. The tag's reflection coefficients are $\Gamma_0 = 1, \Gamma_1 = -1$ and the structural term is $A_s = 0.6047 + j0.5042$ (realistic antenna value from [13], [29]). The figure depicts the *average* BER for each modulation after 500,000 experiments. For each experiment, random channel and carrier phases are generated, and CFO is considered steady for only a small number of consecutive bits ($N = 50$). Three different scenarios are presented, for three values of the emitter-to-reader channel factor: $a_{\text{CR}} = 0.4$, $a_{\text{CR}} = 0.01$, and $a_{\text{CR}} = 0$.

Interestingly, it is observed that for OOK, as the emitter-to-reader channel factor drops (i.e. more attenuation), the BER drops faster. This is due to the BER averaging; recall from Eq. (39) that the SNR for OOK depends on the quantities a and b which are the magnitude values of the noiseless component of Eq. (33). These values vary randomly among the experiments due to the random channel phases they incorporate, and thus the SNR varies also. There are phase combinations that will cause the SNR of Eq. (39) to drop, which leads to (average) BER degradation.[4]

That is not the case for FSK. Notice that for the latter, the BER performance is the same for any channel factor a_{CR}. Thus, FSK is a more robust communication scheme

[4]If one thinks the values in Eq. (33) as vectors on the complex plane, for certain (random) phases, antipodal vectors may occur that cancel out, thus yielding a small magnitude vector. This reflects to a small value of a, and thus, a small CSR.

for the backscatter link, as it is immune to the channel conditions changes. Moreover, FSK fits perfectly to the concept of backscatter sensor networks, since it accounts for multiple access via frequency division multiplexing (FDM). Each sensor occupies specific, predefined subcarriers and does not collide with other sensors. Thanks to the low bitrate, the bandwidth for each sensor is very narrow, which allows many tags to be fitted in a given frequency band. FSK however, requires extra processing for CFO estimation which can be an intensive task if high FFT resolution is desired. Nevertheless, it is still preferred over OOK (which requires no intensive processing for CFO compensation), because of the "stable" BER performance at different channel conditions.

VI. Achieved Ranges

Range measurements were conducted outdoors with a bistatic scatter radio setup. An RF tag was set to modulate data using the FSK modulation scheme, at 1kbps bitrate. A carrier emitter, with +13dBm transmit power at 867MHz, was used to illuminate the tag. The whole reception and signal processing was done with a *commodity* USRP software defined radio and a PC running custom receiver scripts. The maximum BER value measured was 5%, which for the low-bitrate scenario examined corresponds to exactly 1 erroneous bit in a packet of $N = 20$ bits in total. It is noted that all the antennas were omnidirectional on the emitter, tag, and reader. In Fig. 12 four different setups are presented, with their corresponding measurements. First, a tag is placed at the vicinity of the carrier emitter for different given emitter-to-reader distances. Next, the tag is again placed at the vicinity of the carrier emitter, in a way that the tag-to-reader distance is longer than the emitter-to-reader distance. Then, the tag is placed at the vicinity of the reader. Finally, a triangle topology is tested so as to fully characterize the effective range performance on a field.

The results are more than encouraging. For an emitter-to-reader distance of more than 134 meters, a tag may be successfully decoded up to 4 meters away from the emitter. In the uppermost table (Fig. 12), it can be seen that as the emitter-to-reader distance decreases, the tags can be decoded successfully at much longer distances. As an example, for an emitter-to-reader distance of 48 meters, tags my be decoded successfully at 16 meters away from the emitter. In the second table, it can be seen that the tag may reach up to 14 meters *behind* the emitter for the same emitter-to-reader distance. The aforementioned essentially mean that tags are successfully decoded in an elliptical-like cell around the carrier emitter. For the same topology, when the tag is closer to the reader, ranges of up to 24 meters have been reported (third table). Finally, in a triangle topology, with an emitter-to-reader distance of 100 meters, an emitter-to-tag distance of 5.5 meters can be achieved. When the emitter-to-reader distance is reduced to 48 meters, the emitter-to-tag distance may reach up to 16 meters (fourth table).

The measurements show that large-area cells may be formed at relatively long distances from the reader, and these cells' diameter grows as the emitters approach the reader. The aforementioned justify the concept of cellular backscatter

Tag close to Carrier Emitter

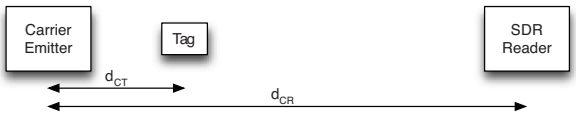

Emitter to SDR dist. d_{CR}	Emitter to Tag dist. d_{CT}	BER
$>$ 134 m	2 m	0%
	4 m	5%
118 m	4 m	0%
	6 m	5%
84 m	8 m	0%
	10 m	5%
48 m	15 m	0%
	16 m	1%

Tag behind Carrier Emitter

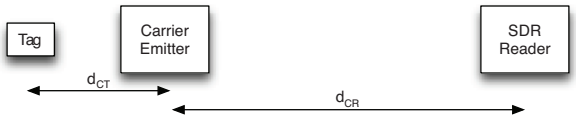

Emitter to SDR dist. d_{CR}	Emitter to Tag dist. d_{CT}	BER
48 m	12 m	0%
	14 m	5%

Tag close to Reader

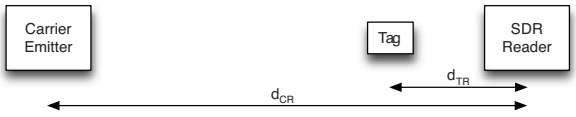

Emitter to SDR dist. d_{CR}	SDR to Tag dist. d_{TR}	BER
48 m	17 m	0%
	24 m	2%

Triangle Topology

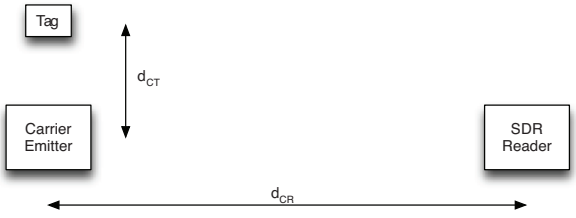

Emitter to SDR dist. d_{CR}	Emitter to Tag dist. d_{CT}	BER
100 m	3.5 m	0%
	5.5 m	5%
84 m	7.5 m	1%
	10 m	5%
48 m	15.5 m	3%
	16.5 m	5%

Fig. 12. Achieved ranges for several bistatic setups.

architectures, where multiple carrier emitters may be placed on a field to form carrier-illuminated cells where tags reside. By strategically placing the carrier emitters, a scatter radio network can be formed and a large field coverage can be achieved, with only one reader.

There is rich prior art research for multiple access schemes in such scatter radio networks. Since each tag in a cell can be allocated its own, unique subcarriers, FDM can be achieved among the tags in a cell. Theoretical analysis in [30] studies the impact of randomly allocating the tag subcarrier frequencies in such an FDM scenario. The outage probability can be calculated given the number of tags in a cell. To avoid interference between adjacent cells, the carrier emitters shall utilize a time division multiplexing (TDM) scheme. This is made possible if the carrier emitters come in the form of low-cost WSN nodes that can be coordinated centrally by the reader. In that way, the cells may be activated in a round-robin manner to read each cell's tags. The concept of the FDM scheme is described in [31], [32]. In those works, a first of a kind backscatter sensor network (BSN) is demonstrated, where the sensors utilize analog frequency modulation (FM), in contrast with this work, where digital FSK modulation was presented. Nevertheless, that FDM scheme perfectly applies for both analog FM and the digital FSK scatter radio communication scheme presented in this paper.

VII. Conclusion

This work presented the bistatic scatter radio system, which can be utilized to build large scale low-cost and low-power backscatter sensor networks with extended field coverage. The complete signal model was derived for the bistatic link, taking into account important tag microwave parameters. Two tag modulation schemes for information transmission were presented (OOK and FSK) and receivers were derived for both. The proposed receivers were characterized in terms of BER performance and the two modulation schemes were compared under different channel conditions. It was shown that a tag and its corresponding receiver are tied together and should be cross-designed to ensure performance maximization, contrary to common belief in the backscatter/RFID field. All parameters should be taken into account while designing scatter radio tags, combining knowledge from the electromagnetics field (antenna load selection, antenna structural mode) and the communication field (tag modulation scheme, receiver processing). Experimentation for the proposed system was conducted with commodity SDR, to test range performance of the bistatic architecture. Ranges of more than 130 meters were achieved (at +13dBm transmission power), demonstrating that ultra-simple, single transistor front-ends are feasible for low bitrate communication. Thus, bistatic scatter radio can be regarded as a key technology enabler for large-scale, ultra low-cost and low-power WSNs.

References

[1] H. Stockman, "Communication by means of reflected power," *Proc. IRE*, pp. 1196–1204, Oct. 1948.

[2] *EPC Radio-Frequency Identity Protocols, Class-1 Generation-2 UHF RFID Protocol for Communications at 860MHZ–960MHZ, version 1.2.0*. EPC Global, 2008.

[3] G. Vannucci, A. Bletsas, and D. Leigh, "A software-defined radio system for backscatter sensor networks," *IEEE Trans. Wireless Commun.*, vol. 7, no. 6, pp. 2170–2179, Jun. 2008.

[4] A. Sample, D. Yeager, P. Powledge, and J. Smith, "Design of a passively-powered, programmable sensing platform for UHF RFID systems," in *IEEE Intl. Conf. on RFID 2007*, Grapevine, TX, Mar. 2007, pp. 149–156.

[5] V. Lakafosis, A. Rida, R. Vyas, L. Yang, S. Nikolaou, and M. M. Tentzeris, "Progress towards the first wireless sensor networks consisting of inkjet-printed, paper-based RFID-enabled sensor tags," *Proc. IEEE*, vol. 98, no. 9, pp. 1601–1609, Sep. 2010.

[6] J. Kimionis, A. Bletsas, and J. N. Sahalos, "Design and implementation of RFID systems with software defined radio," in *6th IEEE European Conf. on Antennas and Propagation (EuCAP)*, Prague, Czech Republic, Mar. 2012, pp. 3464–3468.

[7] D. M. Dobkin, *The RF in RFID: Passive UHF RFID in Practice*. Newnes (Elsevier), 2008.

[8] J. D. Griffin and G. D. Durgin, "Complete link budgets for backscatter-radio and RFID systems," *IEEE Antennas Propagat. Mag.*, vol. 51, no. 2, pp. 11–25, Apr. 2009.

[9] D. Tse and P. Viswanath, *Fundamentals of Wireless Communication*. Cambridge University Press, 2005.

[10] D. Kim, M. A. Ingram, and W. W. Smith Jr., "Measurements of small-scale fading and path loss for long range RF tags," *IEEE Trans. Antennas Propagat.*, vol. 51, no. 8, pp. 1740–1749, Aug. 2003.

[11] U. Karthaus and M. Fischer, "Fully integrated passive UHF RFID transponder IC with 16.7μW minimum RF input power," *IEEE J. Solid-State Circuits*, pp. 1602–1608, Oct. 2003.

[12] P. Nikitin, K. V. S. Rao, S. Lam, V. Pillai, R. Martinez, and H. Heinrich, "Power reflection coefficient analysis for complex impedances in RFID tag design," *IEEE Trans. Microwave Theory Tech.*, vol. 53, no. 9, pp. 2721–2725, Sep. 2005.

[13] A. Bletsas, A. G. Dimitriou, and J. N. Sahalos, "Improving backscatter radio tag efficiency," *IEEE Trans. Microwave Theory Tech.*, vol. 58, no. 6, pp. 1502–1509, Jun. 2010.

[14] C. He and Z. J. Wang, "Closed-form BER analysis of non-coherent FSK in MISO double rayleigh fading/RFID channel," *IEEE Communications Letters*, vol. 15, no. 8, pp. 848–850, 2011.

[15] C. He, X. Chen, Z. J. Wang, and W. Su, "On the performance of MIMO RFID backscattering channels," *EURASIP Journal on Wireless Communications and Networking*, vol. 2012, no. 1, pp. 1–15, 2012.

[16] J. D. Griffin and G. D. Durgin, "Gains for RF tags using multiple antennas," *IEEE Trans. Antennas Propagat.*, vol. 56, no. 2, pp. 563–570, Feb. 2008.

[17] ——, "Multipath fading measurements at 5.8 GHz for backscatter tags with multiple antennas," *IEEE Trans. Antennas Propagat.*, vol. 58, no. 11, pp. 3693–3700, Nov. 2010.

[18] A. Sample, J. Braun, A. Parks, and J. Smith, "Photovoltaic enhanced UHF RFID tag antennas for dual purpose energy harvesting," in *IEEE Intl. Conf. on RFID 2011*, Orlando, FL, Apr. 2011, pp. 146–153.

[19] D. D. Donno, F. Ricciato, L. Catarinucci, A. Coluccia, and L. Tarricone, "Challenge: Towards distributed RFID sensing with software-defined radio," in *16th Annual Intl. Conf. on Mobile Computing and Networking (ACM MobiCom)*, Chicago, IL, 2010, pp. 97–104.

[20] M. Buettner and D. Wetherall, "A 'Gen 2' RFID monitor based on the USRP," *ACM SIGCOMM Computer Communication Review*, vol. 40, no. 3, pp. 42–47, Jul. 2010.

[21] V. Liu, A. Parks, V. Talla, S. Gollakota, D. Wetherall, and J. R. Smith, "Ambient backscatter: Wireless communication out of thin air," in *ACM SIGCOMM 2013*, Hong Kong, China, 2013, pp. 39–50.

[22] S. Thomas, E. Wheeler, J. Teizer, and M. Reynolds, "Quadrature amplitude modulated backscatter in passive and semipassive UHF RFID systems," *IEEE Trans. Microwave Theory Tech.*, vol. 60, no. 4, pp. 1175–1182, Apr. 2012.

[23] C. A. Balanis, *Antenna Theory: Analysis and Design*, 3rd ed. New Jersey: John Wiley and Sons, 2005.

[24] J. Kimionis, "Bistatic scatter radio for increased-range environmental sensing," M.S. Thesis, Technical University of Crete, 2013, supervisor A. Bletsas.

[25] M. K. Simon, *Probability Distributions Involving Gaussian Random Variables: A Handbook for Engineers and Scientists*. New York, NY, 10013: Springer Science and Business Media LLC, 2002.

[26] J. G. Proakis, *Digital Communications*, 4th ed. New York, NY, 10020: McGraw-Hill, Inc., 2001.

[27] M. Abramowitz and I. A. Stegun, *Handbook of Mathematical Functions wih Formulas, Graphs, and Mathematical Tables*. Washington, D.C.: United States Department of Commerce, 1970.

[28] J. G. Proakis and M. Salehi, *Communication Systems Engineering*, 2nd ed. Prentice-Hall, 2002.
[29] C.-C. Yen, A. E. Gutierrez, D. Veeramani, and D. van der Weide, "Radar cross-section analysis of backscattering RFID tags," *IEEE Antennas and Wireless Propagation Letters*, vol. 6, pp. 279–281, 2007.
[30] A. Bletsas, S. Siachalou, and J. N. Sahalos, "Anti-collision backscatter sensor networks," *IEEE Trans. Wireless Commun.*, vol. 8, no. 10, pp. 5018–5029, Oct. 2009.
[31] E. Kampianakis, J. Kimionis, K. Tountas, C. Konstantopoulos, E. Koutroulis, and A. Bletsas, "Backscatter sensor network for extended ranges and low cost with frequency modulators: Application on wireless humidity sensing," in *Proc. IEEE Sensors 2013*, Baltimore, MD, Nov. 2013.
[32] E. Kampianakis, S. D. Assimonis, and A. Bletsas, "Network demonstration of low-cost and ultra-low-power environmental sensing with analog backscatter," in *IEEE Topical Conf. on Wireless Sensors and Sensor Networks (WiSNet) 2014*, Newport Beach, CA, Jan. 2014.

John Kimionis (S'10) John Kimionis received his Diploma degree and MSc in Electronic and Computer Engineering from the Technical University of Crete, Greece, in 2011 and 2013, respectively, where he was with the Telecom Lab. He is currently a PhD candidate at the School of Electrical and Computer Engineering, Georgia Institute of Technology, and a research assistant with the ATHENA group. His research interests are in the areas of backscatter radio and RFID, wireless sensor networks, software defined radio for backscatter radio and sensor networks, microwave/RF engineering, telecom modules & algorithms development, and rapid electronics prototyping with inkjet printing and other fabrication technologies. He has received fellowship awards for his undergraduate and graduate studies, and was the recipient of the Second Best Student Paper Award in the IEEE International Conference on RFID-Technologies and Applications (RFID-TA) 2011, Sitges, Barcelona, Spain.

Aggelos Bletsas (S'03–M'05) received with excellence his diploma degree in Electrical and Computer Engineering from Aristotle University of Thessaloniki, Greece in 1998, and the S.M. and Ph.D. degrees from Massachusetts Institute of Technology in 2001 and 2005, respectively. He worked at Mitsubishi Electric Research Laboratories (MERL), Cambridge MA, as a Postdoctoral Fellow and at Radiocommunications Laboratory (RCL), Department of Physics, Aristotle University of Thessaloniki, as a Visiting Scientist. He joined Electronic and Computer Engineering Department, Technical University of Crete, in summer of 2009, as an Assistant Professor, and promoted to Associate Professor at the beginning of 2014. His research interests span the broad area of scalable wireless communication and networking, with emphasis on relay techniques, backscatter communications and RFID, energy harvesting, radio hardware/software implementations for wireless transceivers and low cost sensor networks. His current vision and focus is on single-transistor front-ends and backscatter sensor networks, for LARGE-scale environmental sensing. He is the principal investigator (PI) of project "BLASE: Backscatter Sensor Networks for Large-Scale Environmental Sensing", funded from the General Secretariat of Research & Technology Action "Proposals evaluated positively from the 3rd European Research Council (ERC) Call". He is also Management Committee (MC) member and National Representative in the European Union COST Action IC1301 "Wireless Power Transmission for Sustainable Electronics (WiPE)". He is Associate Editor of IEEE Wireless Communication Letters since its foundation and Technical Program Committee (TPC) member of flagship IEEE conferences. He holds two patents from USPTO and he was recently included in http://www.highlycitedgreekscientists.org/. Dr. Bletsas was the co-recipient of IEEE Communications Society 2008 Marconi Prize Paper Award in Wireless Communications, best paper distinction in ISWCS 2009, Siena, Italy, and Second Best Student Paper Award in the IEEE RFID-TA 2011, Sitges, Barcelona, Spain. Two of his undergraduate advisees were winners of the 2009-2011 and 2011-2012 best Diploma Thesis contest, respectively, among all Greek Universities on "Advanced Wireless Systems", awarded by IEEE VTS/AES joint Greek Chapter. At the end of 2013, Dr. Bletsas was awarded the Technical University of Crete 2013 Research Excellence Award.

John N. Sahalos (M'75–SM'84–F'06–LF'10) received his B.Sc. degree in Physics, in 1967 and his Ph.D degree in Physics, in 1974, from the Aristotle University of Thessaloniki, (AUTH), Greece. Except of his PhD, during 1970-75, he studied at the School of Engineering of AUTH and he received the Diploma (BCE+MCE) in Civil Engineering, (1975). He also, during 1972-74, studied at the School of Science of AUTH and he received the professional Diploma of postgraduate studies in Radio-Electrology, (1975). From 1971 to 1974, he was a Teaching Assistant at the department of Physics, AUTH, and from 1974 to 1976, he was an Instructor there. In 1976, he worked at the ElectroScience Laboratory, the Ohio State University, Columbus, as a Postdoctoral University Fellow. From 1977 to 1986, he was a Professor in the Electrical Engineering Department, University of Thrace, Greece, and Director of the Microwaves Laboratory. From 1986 to 2010, he has been a Professor at the School of Science, AUTH, where he was the director of the postgraduate studies in Electronic Physics and the director of the Radio-Communications Laboratory (RCL). Dr. Sahalos is now Professor at the Electrical & Computer Engineering Department of the University of Nicosia, Cyprus and director of the Radio & Telecommunications Laboratory (RTeLab). During 1981-82, he was a visiting Professor at the Department of Electrical and Computer Engineering, University of Colorado, Boulder. During 1989-90, he was a visiting Professor at the Technical University of Madrid, Spain. He is the author of three books in Greek, of nine book chapters and more than 410 articles published in the scientific literature. He also is the author of the book "The Orthogonal Methods of Array Synthesis, Theory and the ORAMA Computer Tool", Wiley, 2006. His research interests are in the areas of antennas, high frequency techniques, radio-communications, EMC/EMI, RFID, microwaves, and biomedical engineering. Dr. Sahalos is a Professional Engineer and a Consultant to industry. In 2002-04, he was in the Board of Directors of the OTE, the largest Telecommunications Company in Southeast Europe. He served, as a technical advisor, in several national and international committees, as well as, in several Mobile Communications Companies. Since 1992, he has been a member of commissions A and E of URSI. In 1998-2011, he was the president of the Greek committees of URSI. He was the president of the section of Informatics, Telecommunications and Systems of the National Committee of Research and Technology. Dr. Sahalos is a Life Fellow of the IEEE. He also is a member of the Greek Physical Society, an Honor Fellow of Radio-electrology and a member of the Technical Chamber of Greece. He is the creator and leader of an EMC network with five laboratories (3 from the academy and 2 from the industry). He has been honored with a special investigation fellowship of the Ministry of Education & Science, Spain. He also has been honored from several Institutes and Organizations. He has been in the editorial board of three scientific journals. Dr. Sahalos was elected by the department representatives of the Aristotle University of Thessaloniki as the Vice-Chairman of the Research Committee of AUTH for the period 2007-2010. Since 2010, he is the executive manager of the University of Nicosia Research Foundation (UNRF) and a member of the consulting committee of the GRNET S.A. Dr. Sahalos is a member of EuRAAP as a delegate of Cyprus, Greece, Israel & Turkey. He has supervised 31 PhDs and more than 100 postgraduate diploma theses. With his colleagues Prof. Sahalos designed several well known innovative products like the Electric Impedance Tomography (EIT), the Microwave Landing System (MLS), the ORAMA simulator and the SMS-K monitoring system.